

Strain Distribution of Basalt FRP-Wrapped Concrete Cylinders

Pedram Sadeghian¹ and Brandon Fillmore

Department of Civil and Resource Engineering, Dalhousie University, Halifax, NS, B3H 4R2, Canada.

ABSTRACT

This paper presents the results of an experimental study on the distribution of strain on a unidirectional basalt fiber-reinforced polymer (FRP) wrapped around concrete cylinders. A total of 12 cylinders (150 mm x 300 mm) were wrapped with 2, 4, and 6 layers of basalt FRP (BFRP) and the distribution of hoop strain under axial compression load was studied using multiple strain gauges. The new aspect of this study is the use of BFRPs as a new construction material for wrapping concrete elements with a focus on the distribution of hoop strain towards refining design strain of the wrap. Also, the effect of number of BFRP layers on the premature rupture of the wrap with respect to flat coupon test was evaluated in the form of a strain efficiency factor. It was concluded that the maximum hoop strain was not necessarily associated with the ruptured areas of the wrap. Also, an analysis of variances showed that the difference between hoop strains in the overlap and non-overlap regions was non-significant and an average hoop strain can represent the overall dilation of the specimens. The average strain efficiency factor was found ranging from 0.61 to 0.86. The test data was added to a large database of concrete cylinders wrapped with unidirectional FRPs and after statistical evaluations a refined strain efficiency factor of 0.70 was proposed instead of the current factor of 0.55 in ACI 440.2R-17 for design applications.

KEYWORDS: Strain efficiency; fiber-reinforced polymer; basalt; confinement; rupture.

<https://doi.org/10.1016/j.cscm.2018.e00171>

¹ Corresponding Author: Pedram.Sadeghian@dal.ca

23 **1. INTRODUCTION**

24 During the past three decades, the use of externally bonded fiber-reinforced polymer (FRP)
25 composites for strengthening existing reinforced concrete (RC) columns have been extensively
26 investigated [1][2][3][4][5]. Unidirectional FRP wraps made of carbon [6][7][8][9][10], glass
27 [11][12][13], and aramid [14][15][16] have been typically applied in the circumferential (i.e. hoop)
28 direction of circular cross-section of concrete specimens and tested under axial compression.
29 Recently, basalt fibers have gained increasing attention as FRP materials for strengthening
30 applications especially as an alternative to glass fibres (typically E-glass) [17][18][19].

31 Basalt is a natural, hard, dense, dark brown to black volcanic rock originating at a depth of
32 hundreds of kilometers beneath the earth and reaching the surface as molten magma [20]. The
33 current production technology for continuous basalt fibres is very similar to that used for E-glass
34 fibers. The main difference is that E-glass is made from a complex batch of materials whereas
35 basalt filament is made from melting basalt rock with no other additives. The simplicity of the
36 manufacturing process reduces the production cost of basalt fibers [21]. As the production process
37 does not require additives and a lower amount of energy is needed, it benefits in terms of
38 environmental impact, economics, and plants' maintenance [22]. The quality and the chemical
39 composition of the raw material have a major effect on cost and properties of basalt fibers and can
40 lead to a broad range of fibres with different mechanical properties [22]. As a result, elastic
41 modulus and strength of basalt FRP (BFRP) composites should be evaluated carefully.

42 Despite of numerous studies on concrete columns/cylinders wrapped with carbon, glass,
43 and aramid FRP (CFRP, GFRP, and AFRP respectively), there is very limited experimental data
44 on BFRP-wrapped concrete. In 2015, Sadeghian and Fam [24] collected a database containing 518
45 cylindrical concrete specimens confined with unidirectional FRPs and later the database was

46 expanded to 774 specimens [22][23]. The database indicated that 68% of the specimens were
47 confined with CFRP, 21% with GFRP, and 11% with AFRP composites. There was no study on
48 unidirectional BFRPs at the time of the study. However, in 2011, Di Ludovico et al. [20]
49 investigated the effectiveness of basalt fibers pre-impregnated with epoxy resin or latex and then
50 bonded with a cement-based mortar (BRM) on concrete cylinders and compared the performance
51 of the system with respect to GFRP wraps. In 2015, Campione et al. [19] studied a balanced
52 bidirectional basalt fabric bonded with epoxy resin (BFRP) to concrete cylinders and tested the
53 specimens under axial compression. The specimens confined with BFRP exhibited strain-
54 softening behavior (after the peak load) with negligible increases in resistance but a significant
55 increase in ultimate strain (up to 5 times the strain at peak load of unconfined concrete). It seems
56 the bidirectional basalt fabric did not have enough stiffness providing minimum required lateral
57 confinement pressure. Despite of the unpromising results, the authors of this paper believe that
58 using unidirectional basalt fabric will provide enough lateral confinement for the concrete core
59 and enhance the performance of the concrete.

60 Recently, Xie and Ozbakkaloglu [26] used unidirectional basalt fabric and made BFRP
61 tubes filled with concrete made of recycled aggregates. Three and five layers of the unidirectional
62 basalt fabric were used and the BFRP tube resulted in a strength gain for the concrete core. The
63 tensile strength and modulus of BFRP coupons were obtained 1584 MPa and 76 GPa, respectively,
64 calculated based on 0.14 mm nominal thickness of dry fabric. More recently, Ouyang et al. [27]
65 presented a comparative study of the seismic behavior of square RC columns retrofitted with CFRP
66 and BFRP sheets. The study demonstrated that the BFRP composites are expected to be a
67 promising alternative to the conventional FRPs (e.g., CFRPs) for the seismic retrofit of square RC
68 columns. The tensile strength and modulus of BFRP coupons were obtained 2048 MPa and 87

69 GPa, respectively, calculated based on 0.17 mm nominal thickness of dry fabric. Further studies
70 were suggested to examine a wider range of FRP stiffness. As discussed, there are very limited
71 studies in the literature on BFRP-confined concrete and there is a gap in the field to fill.

72 At the top of the lack of test data on BFRP-wrapped concrete, the concept of strain
73 efficiency factor [28][29][30] of FRP wraps is still under investigation. Typically, the rupture of
74 FRP in the hoop direction occurs at a strain level less than its rupture strain obtained from flat
75 coupon tests [31][32][33][34][35][36]. The reduced rupture strain is required in most existing
76 confinement models, usually in the form of a strain efficiency factor, as proposed by Pessiki et al.
77 [29], which is the ratio of the reduced rupture strain of the FRP wrap to the rupture strain from flat
78 coupon tests. Lam and Teng [37] calibrated the strain efficiency factor using 52 small-scale
79 concrete cylinders wrapped with CFRPs and computed an average value of 0.59. Harries and Carey
80 [32] computed a value of 0.58 for the strain efficiency factor using a database of 251 test results.

81 Bisby and Take [38] implemented an optical strain measurement technique and found the
82 hoop strain is highly variable over the surface of an FRP-wrapped concrete cylinder and the coupon
83 failure strain can be achieved, although only locally. It was shown that average strain efficiency
84 factors varied between 0.77 and 0.80 for GFRPs and between 0.73 and 1.04 for CFRPs. Sadeghian
85 and Fam [30] showed that strain efficiency factor varied significantly, from 0.12 to 1.22, with an
86 average of 0.67 and a standard deviation of 0.23. The highly variable nature of the hoop strain was
87 also reported by multiple studies [33][39][40]. Despite of numerous studies on parameters
88 affecting the premature FRP rupture, ranging from geometrical discontinuity, triaxial stress states,
89 geometrical imperfections, and non-uniform supports in test setup [28][33][41][42][43][44] there
90 is no mechanics-based theory to consider synergy of all parameters affecting the strain efficiency
91 of FRP-wrapped concrete. As the current strain efficiency factor of 0.55 in ACI 440.2R-17 [45]

92 was proposed in early 2000 based on test data at the time, it is necessary to refine the design factor
93 based on numerous new test data since then and new materials such as BFRPs, which are the
94 subject of this study.

95 This paper presents an experimental study on the distribution of hoop strain on concrete
96 cylinders wrapped with unidirectional BFRPs. Three different number of BFRP layers, namely 2,
97 4, and 6 plies were considered and the specimens were instrumented with multiple strain and
98 displacement gauges to capture axial and hoop strains developed during axial compression tests
99 up to failure. The focus of the study is on the distribution of hoop strain using six strain gauges on
100 the circumference of the wrap at the mid-height of the specimens. The results are compared to the
101 rupture strain of flat coupons in the form of the strain efficiency factor and the significance of the
102 strain variation is evaluated using an analysis of variances. At the end, the results are included in
103 a large database of test data from the literature refining the strain efficiency factor for design
104 applications.

105

106 **2. EXPERIMENTAL PROGRAM**

107 This section presents the details of test matrix, material properties, specimen preparation, test
108 setup, and instrumentation of the test specimens.

109 **2.1. Test Matrix**

110 A total of 12 concrete cylinders with a diameter of 150 mm and a height of 300 mm were prepared.
111 As shown in Table 1, the testing matrix included 4 groups of specimens, namely, plain (control),
112 and wrapped with 2, 4, and 6 layers of BFRPs. Three identical specimens were prepared for each
113 group. For wrapped specimens, a specimen identification (ID) system of LX was selected, where

114 the first part “L” stands for layers and; and the second part “X” stands for the number of BFRP
115 layers, namely 2, 4, and 6.

116 **2.2. Material Properties**

117 Concrete was delivered in a ready-mix batch with maximum aggregate size of 12.7 mm and slump
118 of 100 mm. Due to limitation in the load capacity of the equipment available to the authors, the
119 diameter of the specimens was limited to 150 mm and the maximum aggregate size of 12.7 mm
120 was intentionally selected to be compatible with the size of the specimens. It should be noted that
121 the scale effect is important and should be further studied. The tests on the plain concrete cylinders
122 (150 x 300 mm) showed an average strength of 40.03 MPa ($\pm 1.97\%$) and average corresponding
123 strain of 0.0029 mm/mm ($\pm 4.50\%$). The number in parentheses indicates the coefficient of
124 variation (COV) of the corresponding parameter. The concrete was initially ordered to have a
125 compressive strength of 25 MPa to be representative of a member to be retrofitted, however the
126 ready-mix provider delivered higher strength. It should be highlighted that FRP wraps are more
127 effective on low strength concrete than high strength one. If BFRPs are effective for the strength
128 of about 40 MPa, they will be effective for low strength concrete too.

129 A unidirectional basalt fabric and epoxy resin were used for wrapping the specimens. For
130 resin, a mixture of epoxy resin and slow hardener was used, which reported by manufacturer to
131 have the tensile strength, tensile modulus, and maximum elongation of 50 MPa, 2.8 GPa, and
132 4.5%, respectively. The epoxy resin was reinforced by a unidirectional basalt fabric with the areal
133 weight of 300 g/m². The tensile strength, tensile modulus, and rupture strain of basalt fibers were
134 2100 MPa, 105 GPa, and 2.6%, per manufacturer.

135 Five identical BFRP coupons made of two layers of the unidirectional fabric and epoxy
136 resin were prepared using wet hand lay-up method and tested according to ASTM D3039 [46] in

137 tension. A 100 kN universal testing machine with a displacement rate of 2 mm/min was used. A
138 strain gauge was applied on each side of the coupons, centered in the longitudinal direction of
139 fibers/coupon to measure the axial strain. Figure 1 shows the tensile test results of five identical
140 coupons based on the nominal ply thickness of 0.23 mm. The average tensile strength and elastic
141 modulus of BFRP coupons were obtained 1221.1 MPa ($\pm 2.75\%$) and 48.17 GPa ($\pm 0.32\%$),
142 respectively. It should be highlighted that strain gauges broke at an average strain of 0.016
143 mm/mm. As the coupons were made of unidirectional fabric, the stress-strain curves were extended
144 with the same modulus to the average tensile strength, which was resulted in the rupture strain of
145 0.0253 mm/mm. The linear behavior of the BFRP coupons and calculated rupture strain were
146 further verified using the stroke calibrated with the strain gauge data. Implementation of a non-
147 contact strain measurement method using either laser extensometer or digital image correlation
148 (DIC) is recommended. It should be noted that the elastic modulus was calculated based on strain
149 gauge readings.

150 **2.3. Specimen Preparation**

151 Cylindrical plastic molds with the inner diameter of 150 mm and height of 300 mm were used for
152 the fabrication of concrete specimens. The fresh concrete was placed and consolidated in two
153 layers using scoops, a vibration table, and then the surface was carefully troweled smooth. The
154 consolidated concrete was left in the molds and covered to moist cure for 4 days before the molds
155 were removed and the specimens were relocated to cure and get dry. After at least 28 days, the
156 specimens were cleaned with a wire brush for wrapping procedure. The unidirectional basalt fabric
157 was cut into to the length required for 2, 4, or 6 continuous layers plus a 150-mm overlap extension.
158 The overlap was designed to cover a central angle of 120 degrees. The surface of each concrete
159 specimen was cleaned of dust and covered with a coating of the epoxy resin using a roller. Then

160 the fabric was gradually applied on the wet surface from one end and was saturated from the
161 exterior surface as it was wrapped around the cylinder. After wrapping and saturating were
162 complete, the surface was covered with a wax paper and any air pocket was removed using a
163 metal roller. After 7 days curing at ambient temperature, the wax paper was removed and the top
164 and bottom ends of the specimens were strengthened with two layers of 25 mm wide straps of the
165 same fabric. The straps were applied to prevent any premature failure due to stress concentration
166 at the ends. After curing of the end straps, the specimens were capped with a Sulphur compound
167 for uniform loading. Figure 2 shows some of the specimens after preparation.

168 **2.4. Test Setup and Instrumentation**

169 One specimen per each group of wrapped specimens were instrumented with six hoop strain
170 gauges on the mid-height of the BFRP wrap with 60° central angle apart as shown in Figure 2. The
171 first hoop strain gauge was installed at the middle of overlap region of the wrap ($\theta=0^\circ$) and then
172 the second one at the end of overlap ($\theta=60^\circ$). The rest of hoop strain gauges were installed at 120° ,
173 180° (middle of non-overlap region), 240° , and finally at 300° (the beginning of overlap region).
174 The arrangement was specifically selected to obtain the distribution of hoop strain around the
175 BFRP wrap on both overlap and non-overlap regions. The beginning and end of the overlap were
176 targeted to capture any possible strain concentration due to discontinuity of the wrap. For other
177 two specimens of each group, only two hoop strain gauges were installed at 90° and 270° angles.
178 The specimens were also instrumented with two axial strain gauges, one on the middle of overlap
179 region (0°) and another one on the middle of overlap region (180°) of the BFRP wrap. As shown
180 in Figure 3, all specimens were instrumented with two displacement gauges along the axial
181 direction of the specimen to measure average strain over 150 mm gauge length as a backup for the
182 axial strain gauges. The plain specimens were instrumented with two lateral displacement gauges

183 in the radial directions at 90° and 270° angles in addition to the axial ones. A 2 MN universal
184 testing machine was used for testing with 0.6 mm/min displacement control loading rate. In
185 addition to the strain and displacement gauges, the load and stroke were also collected by a data
186 acquisition system at the rate of 10 data points per second.

187

188 **3. TEST RESULTS AND DISCUSSION**

189 This section presents the details of failure mode, effectiveness of BFRP wraps, stress-strain
190 behavior, hoop strain distribution, strain efficiency factor, and refinement of strain efficiency
191 factor for design applications.

192 **3.1. Failure Mode**

193 Figure 4 shows the specimens after failure. At the early stages of loading of the wrapped
194 specimens, the noise related to the micro-cracking of concrete core was evident, indicating the
195 start of stress transfer from the dilated concrete to the wrap. Prior to the failure, cracking noises
196 were frequently heard. The failure pattern of BFRP-wrapped specimens was predominately due to
197 hoop rupture of the wrap in the non-overlap region. For the specimens wrapped with two layers of
198 BFRP (L2 specimens), the rupture of hoop fibers was gradually progressed up to a point that
199 significant amount of the wrap was ruptured and the load dropped suddenly. With increasing the
200 number of layers to four (L4) and six (L6) layers, the rupture of hoop fibers occurred in a shorter
201 amount of time and the failure was more sudden with an explosive noise. Overall, the failure was
202 controlled with rupture of the BFRP wrap in the non-overlap region around the mid-height of the
203 specimens. Compared to the first author's previous observations on CFRP-wrapped cylinders [47],
204 the failure of BFRP-wrapped cylinders was less explosive. This can be explained by lower
205 modulus and strength of BFRPs than CFRPs and the fact that less energy was released at the time

206 of failure. At the same time, the strength gain was significant as it is discussed in the following
207 section.

208 **3.2. Effectiveness of BFRP Wraps**

209 The test results of BFRP-wrapped specimens are summarized in Table 2. The results show an
210 average confined concrete strength (f'_{cc}) of 56.27 MPa ($\pm 0.79\%$), 76.98 MPa ($\pm 1.43\%$), and 94.57
211 MPa ($\pm 5.17\%$) for the specimens wrapped with 2, 4, and 6 layers of BFRPs, respectively. It
212 indicates that wrapping concrete cylinders with 2, 4, and 6 layers of BFRP increased the
213 compressive strength of plain concrete with a factor of 1.41, 1.92, and 2.36; respectively. Similarly,
214 the results show an average confined concrete strain (ϵ_{cc}) of 0.0080 mm/mm ($\pm 5.22\%$), 0.0200
215 mm/mm ($\pm 3.03\%$), and 0.0238 mm/mm ($\pm 16.23\%$) for the specimens wrapped with 2, 4, and 6
216 layers of BFRPs, respectively. It means wrapping the plain concrete cylinders with 2, 4, and 6
217 layers of BFRPs increased the strain of plain concrete at peak load with a factor of 2.77, 6.95, and
218 8.25; respectively. As expected, FRP wrapping increased strain with higher rate than strength. It
219 should be highlighted that only 4 layers of unidirectional basalt fabric with areal weight of 300
220 gsm/layer wrapped around a standard concrete cylinder with an epoxy resin almost doubled the
221 strength of concrete. This indicates the effectiveness of BFRP composites for strengthening
222 applications.

223 **3.3. Stress-Strain Behavior**

224 Figure 5 shows the stress–strain behavior of all specimens. Overall, the stress-strain curves of the
225 wrapped specimens can be considered in three zones. In the first zone, the behavior of the wrapped
226 concrete is mostly linear and similar to the plain concrete. In the second zone, as the concrete core
227 dilates and the wrap is activated, the wrap is stretched and a tension stress in the wrap and a
228 confinement stress on the concrete core are induced. In the third zone, because of large dilation,

229 the wrap is fully activated and the confinement stress increases proportional to the stiffness of the
230 wrap. The first and third zones are almost linear and the second zone is non-linear.

231 The axial strain on the right side of horizontal axis in Figure 5 was calculated based on
232 average of two axial strain gauges installed on the BFRP wrap. The hoop strain on the left side of
233 the horizontal axis was also calculated on average of all hoop strain gauges installed on the BFRP
234 wrap. It should be noted that the axial strain of each specimen was also calculated from the axial
235 displacement gauges and the results showed very good agreement with that of strain gauges. As
236 the displacement gauges were bonded to the wrap using an adhesive and some of them were
237 deboned before the ultimate load, the axial strains reported in this study are only based on the
238 strain gauge data to be consistent for all specimens.

239 As shown in Figure 5, it can be observed that as the number of BFRP layers increases, the
240 third zone slope increases to a point with higher stress and strain. However, the average hoop
241 rupture strain does not increase. The distribution of hoop strain will be discussed more in depth in
242 the following sections. Overall, all three identical specimens of each group resulted in almost
243 identical stress-strain curve, which indicates the consistency of test results.

244 **3.4. Volumetric Strain and Dilation**

245 Figure 6 presents the variation of axial stress vs. volumetric strain of the specimens. The
246 volumetric strain (ε_v) was calculated as follows:

$$\varepsilon_v = \varepsilon_a + 2\varepsilon_h \quad (1)$$

247 where ε_a is the average axial strain and ε_h is the average hoop strain. As shown in the figure, the
248 first zone of curves is linear and indicates an increasing negative volumetric strain (i.e. volume
249 compaction) as axial stress increases. At a certain point, the behavior changes and volumetric strain
250 starts to increase, which can be considered the beginning of the second zone (i.e. transition zone).

251 When volumetric strain becomes zero (i.e. volume of cylinder equals to initial volume), the third
252 zone can be considered to begin. At this point the wrap is fully activated as the specimen enters to
253 volume expansion. The specimens with 2 BFRP layers experienced a fast rate of volume expansion
254 with a shallow third zone, which indicate the low stiffness of the wrap. As the number of BFRP
255 layers increases, the slope of the third zone increases showing a significant gain of strength. In
256 order to characterize the dilation properties of the specimens, dilation rate (μ) of each specimen
257 can be calculated as follows:

$$\mu = \frac{\Delta\varepsilon_h}{\Delta\varepsilon_a} \quad (2)$$

258 where $\Delta\varepsilon_a$ is the change of average axial strain and $\Delta\varepsilon_h$ is the change of average hoop strain. The
259 dilation rate was calculated based on the ratio of the slope of a line fitted into the axial strain for
260 10 adjacent data points to that of the hoop strains rather than using only 2 adjacent data points to
261 filter localized noises. Figure 7 shows the variation of dilation rate vs. axial strain of the specimens.
262 Technically, the dilation rate is the Poisson's ratio of concrete at the first zone of stress-strain curve
263 (i.e. linear behavior). Then, as the axial strain increases, the dilation rate increases almost
264 exponentially. For plain specimens, the dilation rate approaches to infinity, which means crushing
265 and spalling of concrete. For BFRP-wrapped specimen, the dilation rate reaches to a peak point
266 and then decreases. It seems the axial strain corresponding the peak dilation rate corresponds to
267 the strain of plain concrete at peak load. As the number of BFRP layers increases, the peak dilation
268 rate decreases. As shown in Figure 7, the dilation rate of the specimens with 6 BFRP layers reaches
269 a peak of about 1.25 and then decreases and stabilizes at an ultimate value of 0.5 which is Poisson's
270 ratio of elastoplastic materials in the plastic region. The same trend can be seen for the specimens
271 with 4 BFRP layers with a peak of about 1.75 and then an ultimate value of 1.0. The specimens
272 with 2 BFRP layers show a peak dilation rate of about 4.0 and then it decreases to an ultimate

273 value of about 2.0. The figure indicates that both peak and ultimate dilation rates depend on the
274 number of BFRP layers (i.e. the wrap stiffness). Figure 8 shows the variation of hoop strain vs.
275 axial strain of the specimens. All specimens exhibit an initial linear behavior with Poisson's ratio
276 of about 0.2 and then with a nonlinear transition zone, the BFRP-wrapped specimens approach to
277 a constant slope. The specimens wrapped with 4 and 6 BFRP layers approach to almost similar
278 direction, but the specimens with 2 BFRP layers show a different direction. Overall, 4 and 6 layers
279 of BFRP wraps were effective to control the dilation rate of concrete leading to a quasi-plastic
280 behavior.

281 **3.5. Hoop Strain Distribution**

282 The focus of this paper is on the distribution of hoop strain on BFRP wrap. Figure 9 presents the
283 variation of hoop strain vs. central angle at mid-height of the specimens as axial stress increases
284 from a fraction of f'_{cc} to full f'_{cc} . The overlap region is also shaded in the figure. As shown in
285 Figure 9(a), when the axial stress of specimen L2-1 is as low as 50 MPa (i.e. $0.89 f'_{cc}$), the hoop
286 strain has an almost uniform distribution. As axial stress increases, the hoop strain increase in a
287 non-uniform pattern with a higher rate of increase in the non-overlap region. The non-uniform
288 pattern with a peak at 180° (i.e. middle of non-overlap region) continues, until the wrap ruptures
289 at the peak hoop strain of 0.0186 mm/mm, which is less than the rupture tensile strain of 0.0253
290 mm/mm corresponding to the flat coupon tests presented in Figure 1. Table 2 presents the peak
291 strain comparing to the average of all strain gauges plus the average of strain gauges in the overlap
292 and non-overlap regions.

293 Similarly, Figure 9 (b) and (c) present the variation of hoop strain for specimen L4-1 and
294 L6-1, respectively. As shown, when the axial stress of the specimen is as low as 50 MPa (i.e. 0.65
295 f'_{cc} for L4-1 and $0.53 f'_{cc}$ for L4-1), the hoop strain has an almost uniform distribution. As axial

296 stress increases, the hoop strain of L4-1 and L6-1 increase in a non-uniform pattern with a higher
297 rate of increase in the non-overlap region. The non-uniform pattern with a peak at 240° and 180°
298 (i.e. almost middle of non-overlap region) continues until the wrap ruptures at the peak hoop strain
299 of 0.0211 and 0.0228 mm/mm, respectively, which is less than the rupture tensile strain of 0.0253
300 mm/mm. Overall, all specimens failed with a peak hoop strain around middle of non-overlap
301 region lower than the rupture strain of flat coupon tests. However, as the number of BFRP layers
302 increased, the peak hoop strain reached closer to the flat coupon rupture strain. Table 2 summarizes
303 the average of all hoop strain gauges, peak hoop strain values, and the ratio of the peak over the
304 average at the peak load of each BFRP-wrapped specimen. It indicates that the average ratio for
305 specimen with 2, 4, and 6 layers of BFRPs is 1.12, 1.08, and 1.14; respectively.

306 Figure 10 shows the effect of number of BFRP layers on distribution of hoop strain at peak
307 load comparing to the average hoop strain of specimen L2, L4, and L6. It seems the number of
308 layer does not affect the overall strain distribution. In order to identify whether or not the number
309 of BFRP layers had a significant effect on the strain distribution, an analysis of variance (ANOVA)
310 was performed. ANOVA allows a comparison of the variance caused by the between-groups
311 variability (mean square effect or MS_{effect}) with the within-group variability (mean square error or
312 MS_{error}) by means of the F-test. The analysis results are presented in an F-value as follows:

$$F = \frac{MS_{effect}}{MS_{error}} \quad (3)$$

313 The ANOVA analysis tests whether the F-value is significantly greater than a critical value
314 F_{crit} , extracted from the distribution of statistical tables based on the number of degrees of freedom.
315 A test result (calculated from the null hypothesis and the sample) is called statistically significant
316 if it is deemed unlikely to have occurred by chance, assuming the truth of the null hypothesis. A

317 statistically significant result justifies the rejection of the null hypothesis. In this study, a one-way
318 ANOVA using a confidence level of 95% (significance level of 0.05) was performed.

319 Considering the hoop strains recorded from six strain gauges of the first specimen of each
320 group, the ANOVA analysis shows that the results are non-significant at the 5% significance level
321 ($F=2.59 < F_{crit}=3.11$), which accepts the null hypothesis, concluding that the variation of hoop strain
322 of BFRP wraps around the concrete cylinders tested in this study is non-significant at the 5%
323 significance level. In addition, the effect of number of BFRP layers on variation of hoop strain is
324 also considered non-significant since $F=1.15 < F_{crit}=3.68$. As a result, using the average hoop strain
325 instead of peak hoop strain is justifies. To support further this conclusion, Figure 11 shows the
326 ruptured areas of BFRP wraps compared with hoop strain distribution of the wraps at peak load.
327 The figure indicates that the peak strain is not necessary in the ruptured area. It can be concluded
328 that the variation of hoop strain is localized and is not associated with the ruptured areas of BFRP
329 wraps considered in this study. Further study on other FRP materials is needed to generalize this
330 conclusion.

331 **3.5. Strain Efficiency Factor**

332 In order to quantify the premature rupture of BFRP wraps with respect to flat coupon test result,
333 the strain efficiency factor (κ_ε) of each specimen was calculated as follows:

$$\kappa_\varepsilon = \frac{\varepsilon_{h,rupt}}{\varepsilon_{fu}} \quad (4)$$

334 where $\varepsilon_{h,rupt}$ is the hoop strain in the FRP wrap at failure and ε_{fu} is the flat coupon's rupture strain
335 in tension. Using the equation, the strain efficiency factor of each specimens was calculated and
336 presented in Table 3. For comparison, the factor was calculated using both average hoop strain and
337 peak hoop strain. The strain efficiency factor based on average hoop strain ranges from 0.61 to
338 0.86 with an average of 0.72 ($\pm 10.48\%$). The strain efficiency factor based on peak hoop strain

339 ranges from 0.65 to 0.90 with an average of 0.78 ($\pm 10.78\%$). The ANOVA analysis shows that
340 there is a non-significant difference between the strain efficiency factor based on average and peak
341 hoop strains ($F=2.87 < F_{crit}=4.49$). As a result, the strain efficiency factor based on average hoop
342 strain can be used for further analyses of the specimens tested in this study. The ANOVA analysis
343 also shows that there is a non-significant difference between the strain efficiency factor of the
344 specimens wrapped with 2, 4, and 6 BFRP layers ($F=2.55 < F_{crit}=5.14$). It means strain efficiency
345 factor is not dependent on the thickness of the BFRP wrap. There is no in-depth study in the
346 literature on the effect of FRP wrap thickness on strain efficiency factor. Thus, more research is
347 needed using other FRP materials to generalize this conclusion.

348 **3.6. Refining Design Strain Efficiency Factor**

349 The concept of strain efficiency factor κ_ϵ has been implemented by the American Concrete Institute
350 in ACI 440.2R-17 [45] which is the well-known guide for the design and construction of externally
351 bonded FRP systems for strengthening concrete structures as follows:

$$\epsilon_{fe} = \kappa_\epsilon \epsilon_{fu} \quad (5)$$

352 where ϵ_{fe} is the effective strain in FRP reinforcement attained at failure, ϵ_{fu} is the design rupture
353 strain of FRP reinforcement, and κ_ϵ is equal to 0.55 per ACI 440.2R-17. The design guide offered
354 some speculations on the reasons behind the reduction observed experimentally, including the
355 multi-axial state of stress in the jacket, compared to the uniaxial state of stress in coupons.
356 However, no rational approach was offered to express the hypothesis. Multiple studies have been
357 performed to rationalize strain efficiency factor, however the complexity of the mechanics of the
358 problem and the synergic effects of multiple parameters on the premature rupture of FRP wraps
359 have made the problem too complicated to be solved completely. At this stage, the approach of
360 ACI 440.2R-17 proposing a constant value based on experimental data seems more applicable for

361 practicing engineers. The current design strain efficiency factor κ_ϵ of 0.55 was calibrated in early
 362 2000 by Lam and Teng [37] and Harries and Carey [32] using 52 and 251 concrete cylinders
 363 wrapped with FRPs, respectively. As numerous test data has been produced in the past 15 years, a
 364 new calibration is necessary. In order to refine the factor, the test data of this study was added to
 365 the database collected previously [23] by combining two databases [24][25] to form a large
 366 database containing 783 concrete cylinders wrapped with unidirectional FRPs in the hoop direction
 367 resulting an average experimental strain efficiency factor of 0.70 with a standard deviation of 0.25.
 368 To evaluate the effect of the refinement, the FRP confinement model of ACI 440.2R-17 is used.
 369 The model was initially proposed by Lam and Teng [37] as follows:

$$\frac{f'_{cc}}{f'_{co}} = 1 + 3.3 \frac{f_l}{f'_{co}} \quad (6)$$

370 where f'_{cc} is the confined concrete strength, f'_{co} is the unconfined concrete strength, and f_l is the
 371 confining stress defined as:

$$f_l = \frac{2E_f \epsilon_{fe} t}{D} \quad (7)$$

372 where E_f is the elastic modulus of the FRP wrap in the hoop direction, t is the total thickness of the
 373 FRP wrap, D is the diameter of the concrete core, and ϵ_{fe} is the the effective strain defined in Eq.
 374 (5). The confinement model was used to predict the confined concrete strength as presented in
 375 Figure 12. Each circle in the figure represents the coordinate of a data point, where the horizontal
 376 axis is the experimental value and the vertical axis is the predicted value. It is noted that the
 377 fundamental approach to quantify the strain efficiency of FRP wraps is using the compressive
 378 constitutive law of FRP-confined concrete. As it was mentioned earlier, the analysis is complicated
 379 and beyond the scope of this study. The focus of the analytical section of this study is only

380 calibrating the constant strain efficiency factor of ACI 440.2R-17 using its own confinement
381 model.

382 To evaluate the performance of the refined factor, a statistical index known as Root Mean
383 Square Error (RMSE) is implemented. RMSE is the square root of the variance of the residuals
384 which is defined as the following, where n is the number of data points. RMSE indicates how close
385 the predicted values (i.e., y) to the experimental values (i.e., x) as presented is the following
386 equation. Lower values of RMSE indicate a better fit, with zero indicating a perfect prediction that
387 means all data points are located on a 45-degree line.

$$RMSE = \sqrt{\frac{\sum(x - y)^2}{n}} \quad (8)$$

388 As shown in Figure 12, using the experimental strain efficiency factor, the confinement
389 model can predict the experimental f'_{cc} to f'_{co} confining ratio with an RMSE of 0.318. However,
390 using the strain efficiency factor of 0.55, the model underestimates the confining ratio with an
391 RMSE of 0.481. Using the refined strain efficiency factor of 0.70, the data points get slightly closer
392 to the 45-degree line indicating better prediction with an RMSE of 0.402. It means the dispersion
393 degree is slightly enhanced, however there is no significant enhancement. The main point is that
394 using the refined strain efficiency factor of 0.7 does not make the dispersion degree of data points
395 worse than the factor of 0.55, however provides a better frequency distribution as it is discussed
396 later in this section.

397 In addition to the RMSE index, the R^2 index (the square of the correlation coefficient) was
398 computed for each case to evaluate the correlation between the predicted f'_{cc} and experimental f'_{cc} .
399 As shown in Figure 12, the R^2 index between the predicted f'_{cc} and experimental f'_{cc} using the strain
400 efficiency factor of 0.55 and 0.7 is the same ($R^2=0.733$) as changing the constant factor does not

401 change the correlation between the predicted and experimental values. However, using a variable
402 experimental strain efficiency factor, as expected, provides better correlation ($R^2=0.836$). It is
403 important to note that a higher R^2 value does not necessarily indicate a perfect prediction. It only
404 shows that there is a better linear correlation between predicted and experimental values. Thus, the
405 R^2 index is not the best index for the evaluation presented in Figure 12, where RMSE is better
406 suited. Figure 13 presents the variation of RMSE with respect to a range of strain efficiency factors.
407 It clearly indicates that the proposed value of 0.70 for the strain efficiency factor corresponds to
408 the minimum RMSE.

409 Figure 14 shows the frequency distribution of the ratio of predicted f'_{cc} to experimental f'_{cc} .
410 Three strain efficiency factors based on the database (experimental κ_ϵ), ACI 440.2R-17 ($\kappa_\epsilon=0.55$),
411 and the refined factor ($\kappa_\epsilon=0.7$). The histogram was prepared in 30 bins with the width of 0.04. The
412 number of the bins was selected based on the square root of the number of the data points. The
413 figure clearly indicates a better precision using the proposed strain efficiency factor of 0.70 in
414 comparison with the ACI 440.2R-17 strain efficiency factor of 0.55.

415 It can be concluded that the strain efficiency factor in ACI 440.2R-17 can be changed from
416 0.55 to 0.70. It should be noted that this study focused on cylindrical cross-sections, the validity
417 of the performed calibration in case of non-circular cross-sections needs to be tested. There are
418 numerous statistical and analytical studies [48][49][50][51][52] in the literature to extend the
419 analysis presented in this study. Also, a reliability analysis is needed to refine the strength
420 reduction factors (i.e. phi factors) of the design guideline. Moreover, as new FRPs made of
421 polyethylene terephthalate (PET) fibers [53][54], polyethylene naphthalate (PEN) fibers [54], and
422 plant-based fibers [55] and bio-based resins [56] are emerging in the market, the strain efficiency
423 factor needs to be studied more in-depth for new materials and revised accordingly.

424

425 **4. CONCLUSION**

426 This paper presented the results of an experimental study on concrete cylinders wrapped with
427 unidirectional basalt fabrics (300 gsm). Three different number of basalt fiber-reinforced polymer
428 (BFRP) layers, namely 2, 4, and 6 plies were considered and the specimens were instrumented
429 with multiple strain gauges. The results were compared to the rupture strain of flat coupons in the
430 form of a strain efficiency factor. The failure mode, strength gain, dilation, and variation of hoop
431 strain of the specimens were also evaluated. The following conclusions can be drawn from the
432 study:

- 433 • The failure of all specimens wrapped with BFRPs was controlled by the rupture of hoop fibers
434 in the non-overlap region around the mid-height of the specimens. With increasing number of
435 BFRP layers, the rupture of hoop fibers occurred in a shorter time window. In comparison with
436 similar studies on CFRP, the failure of BFRP-wrapped cylinders was less explosive. This can
437 be explained by lower modulus of BFRPs than CFRPs and the fact that less energy was released
438 at the time of failure.
- 439 • Wrapping the plain concrete cylinders with 2, 4, and 6 layers of BFRPs increased the strength
440 with a factor of 1.41, 1.92, and 2.36; respectively. This indicated the effectiveness of basalt
441 fibers for concrete strengthening applications in addition to the other benefits in terms of
442 environmental impact, economics, and plants' maintenance in comparison with fiberglass
443 production.
- 444 • All specimens exhibited a dilation rate with an initial rate of about 0.2 and then with a nonlinear
445 transition zone approaching to a constant rate. The specimens wrapped with 6 BFRP layers

446 approached to an average dilation rate of almost 0.5 indication the effectiveness of BFRP wraps
447 to control dilation rate of concrete leading to a quasi-plastic behavior.

448 • Although the strain of the BFRP wraps in the hoop direction of the cylinders was variable, it
449 was not associated with the ruptured areas of the wrap. An analysis of variances (ANOVA) on
450 three specimens with six hoop strain gauges tested in this study showed that the variation is
451 non-significant at 95% confidence level. In addition, the effect of number of BFRP layers on
452 the variation of hoop strain amongst the three specimens was non-significant. More test results
453 on strain distribution are needed to generalize this conclusion.

454 • The strain efficiency factor of the test specimens based on the average hoop strain ranged from
455 0.61 to 0.86 with an average of 0.72. The strain efficiency factor based on peak hoop strain
456 ranged from 0.65 to 0.90 with an average of 0.78. An ANOVA analysis showed that there is a
457 non-significant difference between the strain efficiency factor based on average and peak hoop
458 strains. As a result, the strain efficiency factor based on average hoop strain was recommended
459 for design applications.

460 • The test data of this study was added to a large database from the literature to form a database
461 containing 783 concrete cylinders wrapped with unidirectional FRPs in the hoop direction
462 resulting an average strain efficiency factor of 0.70 with a standard deviation of 0.25. The
463 strain efficiency factor of 0.70 was proposed instead of the current factor of 0.55 in ACI
464 440.2R-17 design guideline predicting the strength of FRP-wrapped concrete cylinders in the
465 database with the lowest statistical error. It should be noted that a reliability analysis will
466 needed to refine the strength reduction factors (i.e. phi factors) of the design guideline.

467

468 **5. ACKNOWLEDGEMENTS**

469 The authors would like to acknowledge the financial support of NSERC and Dalhousie University.

470

471 **6. CONFLICTS OF INTEREST**

472 None.

473

474 **7. REFERENCES**

475 [1] Bakis C, Bank LC, Brown V, Cosenza E, Davalos JF, Lesko JJ, Machida A, Rizkalla SH,
476 and Triantafillou TC. (2002). Fiber-reinforced polymer composites for construction-state-
477 of-the-art review. *Journal of Composites for Construction*, 6(2), 73-87.

478 [2] Motavalli M, and Czaderski C. (2007). FRP composites for retrofitting of existing civil
479 structures in Europe: state-of-the-art review. *International Conference of Composites &*
480 *Polycon.*, American Composites Manufacturers Association. Tampa, FL, USA.

481 [3] Hollaway LC. (2012). A review of the present and future utilisation of FRP composites in
482 the civil infrastructure with reference to their important in-service properties. *Construction*
483 *and Building Materials*, 24(12), 2419-45.

484 [4] Teng JG, Chen JF, Smith ST, and Lam L. (2003). Behaviour and strength of FRP-
485 strengthened RC structures: a state-of-the-art review. *Proceedings of the institution of civil*
486 *engineers-structures and buildings*, 156(1), 51-62.

487 [5] Nanni, A., and Bradford, N. M. (1995). FRP jacketed concrete under uniaxial
488 compression. *Construction and Building Materials*, 9(2), 115-124.

489 [6] Xiao, Y., and Wu, H. (2000). Compressive behavior of concrete confined by carbon fiber
490 composite jackets. *Journal of materials in civil engineering*, 12(2), 139-146.

- 491 [7] Lam, L., and Teng, J. G. (2004). Ultimate condition of fiber reinforced polymer-confined
492 concrete. *Journal of Composites for Construction*, 8(6), 539-548.
- 493 [8] Berthet, J. F., Ferrier, E., and Hamelin, P. (2005). Compressive behavior of concrete
494 externally confined by composite jackets. Part A: experimental study. *Construction and*
495 *Building Materials*, 19(3), 223-232.
- 496 [9] Cui, C., and Sheikh, S. A. (2010). Experimental study of normal-and high-strength concrete
497 confined with fiber-reinforced polymers. *Journal of Composites for Construction*, 14(5),
498 553-561.
- 499 [10] Micelli, F., and Modarelli, R. (2013). Experimental and analytical study on properties
500 affecting the behaviour of FRP-confined concrete. *Composites Part B: Engineering*, 45(1),
501 1420-1431.
- 502 [11] Jiang, T., and Teng, J. G. (2007). Analysis-oriented stress–strain models for FRP–confined
503 concrete. *Engineering Structures*, 29(11), 2968-2986.
- 504 [12] Almusallam, T. H. (2007). Behavior of normal and high-strength concrete cylinders
505 confined with E-glass/epoxy composite laminates. *Composites Part B: Engineering*, 38(5),
506 629-639.
- 507 [13] Zohrevand, P., and Mirmiran, A. (2011). Behavior of ultrahigh-performance concrete
508 confined by fiber-reinforced polymers. *Journal of materials in civil engineering*, 23(12),
509 1727-1734.
- 510 [14] Silva, M. A., and Rodrigues, C. C. (2006). Size and relative stiffness effects on
511 compressive failure of concrete columns wrapped with glass FRP. *Journal of Materials in*
512 *Civil Engineering*, 18(3), 334-342.

- 513 [15] Rochette, P., and Labossiere, P. (2000). Axial testing of rectangular column models
514 confined with composites. *Journal of composites for construction*, 4(3), 129-136.
- 515 [16] Vincent, T., and Ozbakkaloglu, T. (2013). Influence of fiber orientation and specimen end
516 condition on axial compressive behavior of FRP-confined concrete. *Construction and
517 Building materials*, 47, 814-826.
- 518 [17] Sim, J., and Park, C. (2005). Characteristics of basalt fiber as a strengthening material for
519 concrete structures. *Composites Part B: Engineering*, 36(6), 504-512.
- 520 [18] De Luca, A., Nardone, F., Matta, F., Nanni, A., Lignola, G. P., and Prota, A. (2010).
521 Structural evaluation of full-scale FRP-confined reinforced concrete columns. *Journal of
522 Composites for Construction*, 15(1), 112-123.
- 523 [19] Campione, G., La Mendola, L., Monaco, A., Valenza, A., and Fiore, V. (2015). Behavior
524 in compression of concrete cylinders externally wrapped with basalt fibers. *Composites
525 Part B: Engineering*, 69, 576-586.
- 526 [20] Di Ludovico, M., Prota, A., and Manfredi, G. (2010). Structural upgrade using basalt fibers
527 for concrete confinement. *Journal of composites for construction*, 14(5), 541-552.
- 528 [21] Fiore, V., Di Bella, G. and Valenza, A., 2011. Glass–basalt/epoxy hybrid composites for
529 marine applications. *Materials & Design*, 32(4), pp.2091-2099.
- 530 [22] Fiore, V., Scalici, T., Di Bella, G., and Valenza, A. (2015). A review on basalt fibre and its
531 composites. *Composites Part B: Engineering*, 74, 74-94.
- 532 [23] Keshtegar, B., Sadeghian, P., Gholampour, A., and Ozbakkaloglu, T. (2017). Nonlinear
533 modeling of ultimate strength and strain of FRP-confined concrete using chaos control
534 method. *Composite Structures*, 163, 423-431.

- 535 [24] Sadeghian, P., and Fam, A. (2015). Improved design-oriented confinement models for
536 FRP-wrapped concrete cylinders based on statistical analyses. *Engineering Structures*, 87,
537 162-182.
- 538 [25] Lim, J. C., & Ozbakkaloglu, T. (2014). Design model for FRP-confined normal-and high-
539 strength concrete square and rectangular columns. *Magazine of Concrete Research*, 66(20),
540 1020-1035.
- 541 [26] Xie, T., and Ozbakkaloglu, T. (2016). Behavior of recycled aggregate concrete-filled basalt
542 and carbon FRP tubes. *Construction and Building Materials*, 105, 132-143.
- 543 [27] Ouyang, L. J., Gao, W. Y., Zhen, B., and Lu, Z. D. (2017). Seismic retrofit of square
544 reinforced concrete columns using basalt and carbon fiber-reinforced polymer sheets: A
545 comparative study. *Composite Structures*, 162, 294-307.
- 546 [28] Chen, J. F., Li, S. Q., and Bisby, L. A. (2012). Factors affecting the ultimate condition of
547 FRP-wrapped concrete columns. *Journal of Composites for Construction*, 17(1), 67-78.
- 548 [29] Pessiki, S., Harries, K. A., Kestner, J. T., Sause, R., and Ricles, J. M. (2001). Axial behavior
549 of reinforced concrete columns confined with FRP jackets. *Journal of Composites for*
550 *Construction*, 5(4), 237-245.
- 551 [30] Sadeghian, P., and Fam, A. (2014). A rational approach toward strain efficiency factor of
552 fiber-reinforced polymer-wrapped concrete columns. *ACI Structural Journal*, 111(1), 135-
553 144.
- 554 [31] Chen, J. F., Li, S. Q., Bisby, L. A., and Ai, J. (2011). FRP rupture strains in the split-disk
555 test. *Composites Part B*, 42(4), 962-972.
- 556 [32] Harries, K. A., and Carey, S. A. (2003). Shape and “gap” effects on the behavior of variably
557 confined concrete. *Cement and Concrete Research*, 33(6), 881-890.

- 558 [33] Smith, S. T., Kim, S. J., and Zhang, H. (2010). Behavior and effectiveness of FRP wrap in
559 the confinement of large concrete cylinders. *Journal of Composites for Construction*, 14(5),
560 573–582.
- 561 [34] Bisby, L. A., Dent, A. J., and Green, M. F. (2005). Comparison of confinement models for
562 fiber-reinforced polymer-wrapped concrete. *ACI Structural Journal*, 102(1), 62-72.
- 563 [35] De Lorenzis, L., and Tepfers, R. (2003). Comparative study of models on confinement of
564 concrete cylinders with fiber-reinforced polymer composites. *Journal of Composites for*
565 *Construction*. 7(3), 219-237.
- 566 [36] Xiao, Y., and Wu, H. (2000). Compressive behavior of concrete confined by carbon fiber
567 composite jackets. *Journal of Materials in Civil Engineering*, 12(2), 139-146.
- 568 [37] Lam, L., and Teng, J. G. (2003). Design-oriented stress–strain model for FRP-confined
569 concrete. *Construction and building materials*, 17(6), 471-489.
- 570 [38] Bisby, L. A., and Take, W. A. (2009). Strain localisations in FRP-confined concrete: new
571 insights. *Proceedings of the ICE-Structures and Buildings*, 162(5), 301-309.
- 572 [39] Wu, Y. F., and Jiang, J. F. (2013). Effective strain of FRP for confined circular concrete
573 columns. *Composite Structures*, 95, 479-491.
- 574 [40] El-Hacha, R., and Abdelrahman, K. (2013). Slenderness effect of circular concrete
575 specimens confined with SFRP sheets. *Composites Part B: Engineering*, 44(1), 152-166.
- 576 [41] Vincent, T., and Ozbakkaloglu, T. (2015). Influence of overlap configuration on
577 compressive behavior of CFRP-confined normal-and high-strength concrete. *Materials and*
578 *Structures*, 1-24.

- 579 [42] Pham, T. M., Hadi, M. N., and Youssef, J. (2015). Optimized FRP Wrapping Schemes for
580 Circular Concrete Columns under Axial Compression. *Journal of Composites for*
581 *Construction*, 04015015.
- 582 [43] Fraldi, M., Nunziante, L., Carannante, F., Prota, A., Manfredi, G., and Cosenza, E. (2008).
583 On the prediction of the collapse load of circular concrete columns confined by
584 FRP. *Engineering Structures*, 30(11), 3247-3264.
- 585 [44] Lignola, G. P., Nardone, F., Prota, A., and Manfredi, G. (2012). Analytical model for the
586 effective strain in FRP-wrapped circular RC columns. *Composites Part B:*
587 *Engineering*, 43(8), 3208-3218.
- 588 [45] ACI 440.2R-17 (2017). “Guide for the design and construction of externally bonded FRP
589 systems for strengthening concrete structures.” American Concrete Institute, Farmington,
590 MI, USA.
- 591 [46] ASTM D3039 (2014). “Standard test method for tensile properties of polymer matrix
592 composite materials.” Annual Book of ASTM Standards. West Conshohocken, PA, USA.
- 593 [47] Sadeghian, P., Rahai, A. R., and Ehsani, M. R. (2010). Effect of fiber orientation on
594 compressive behavior of CFRP-confined concrete columns. *Journal of Reinforced Plastics*
595 *and Composites*, 29(9), 1335-1346.
- 596 [48] Rousakis, T., Nistico, N., & Karabinis, A. (2012). Upgraded experimental database of
597 uniformly FRP confined concrete columns for assessment of existing recommendations. In
598 *The 6th International Conference on FRP Composites in Civil Engineering–CICE* (pp. 13-
599 15).
- 600 [49] Yousif, D. S. T. (2013). New model of CFRP-confined circular concrete columns: an
601 approach. *Int J Civil Eng Technol*, 4, 98-110.

- 602 [50] Lim, J. C., Karakus, M., & Ozbakkaloglu, T. (2016). Evaluation of ultimate conditions of
603 FRP-confined concrete columns using genetic programming. *Computers & Structures*,
604 162, 28-37.
- 605 [51] Cascardi, A., Micelli, F., & Aiello, M. A. (2017). An Artificial Neural Networks model for
606 the prediction of the compressive strength of FRP-confined concrete circular columns.
607 *Engineering Structures*, 140, 199-208.
- 608 [52] Mansouri, I., Kisi, O., Sadeghian, P., Lee, C. H., & Hu, J. W. (2017). Prediction of Ultimate
609 Strain and Strength of FRP-Confined Concrete Cylinders Using Soft Computing Methods.
610 *Applied Sciences*, 7(8), 751.
- 611 [53] Pimanmas, A., & Saleem, S. (2018). Dilation Characteristics of PET FRP-Confined
612 Concrete. *Journal of Composites for Construction*, 22(3), 04018006.
- 613 [54] Dai, J. G., Bai, Y. L., & Teng, J. G. (2011). Behavior and modeling of concrete confined
614 with FRP composites of large deformability. *Journal of composites for construction*, 15(6),
615 963-973.
- 616 [55] Wroblewski, L., Hristozov, D., & Sadeghian, P. (2016). Durability of bond between
617 concrete beams and FRP composites made of flax and glass fibers. *Construction and*
618 *Building Materials*, 126, 800-811.
- 619 [56] Mak, K., Fam, A., & MacDougall, C. (2015). Flexural behavior of sandwich panels with
620 bio-FRP skins made of flax fibers and epoxidized pine-oil resin. *Journal of Composites for*
621 *Construction*, 19(6), 04015005.

622

Table 1. Test matrix.

Group #	Group ID	Number of FRP layers	Number of identical specimens
1	Plain	0	3
2	L2	2	3
3	L4	4	3
4	L6	6	3
Total	-	-	12

623

Table 2. Summary of test results.

Specimen ID	Compressive strength f'_{cc} (MPa)	Ultimate axial strain ϵ_{cc} (mm/mm)	Average hoop strain at f'_{cc} (mm/mm)	Peak hoop strain at f'_{cc} (mm/mm)	Peak/average strain ratio
L2-1	55.94	0.0084	0.0159	0.0186	1.17
L2-2	56.09	0.0079	0.0192	0.0222	1.16
L2-3	56.77	0.0076	0.0180	0.0184	1.02
L4-1	76.25	0.0195	0.0183	0.0222	1.21
L4-2	76.44	0.0207	0.0210	0.0213	1.02
L4-3	78.24	0.0199	0.0194	0.0198	1.02
L6-1	95.37	0.0232	0.0179	0.0228	1.27
L6-2	99.01	0.0279	0.0176	0.0178	1.01
L6-3	89.33	0.0202	0.0144	0.0166	1.15

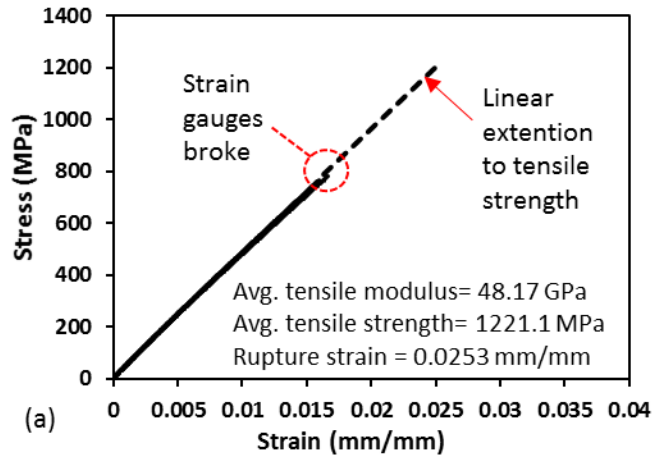
626

Table 3. Comparison of average and peak strain efficiency factor.

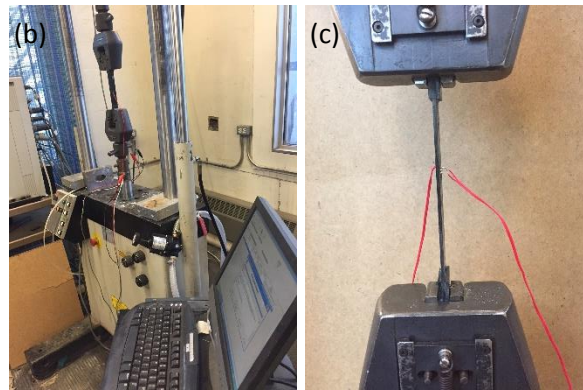
Specimen ID	Average hoop strain (mm/mm)	Average κ_ε	Peak hoop strain (mm/mm)	Peak κ_ε
L2-1	0.0159	0.627	0.0186	0.736
L2-2	0.0193	0.761	0.0222	0.878
L2-3	0.0181	0.716	0.0184	0.729
L4-1	0.0184	0.728	0.0211	0.835
L4-2	0.0219	0.864	0.0213	0.841
L4-3	0.0194	0.769	0.0198	0.783
L6-1	0.0179	0.709	0.0228	0.901
L6-2	0.0176	0.698	0.0178	0.702
L6-3	0.0155	0.612	0.0166	0.655
Average		0.720		0.784

627

628



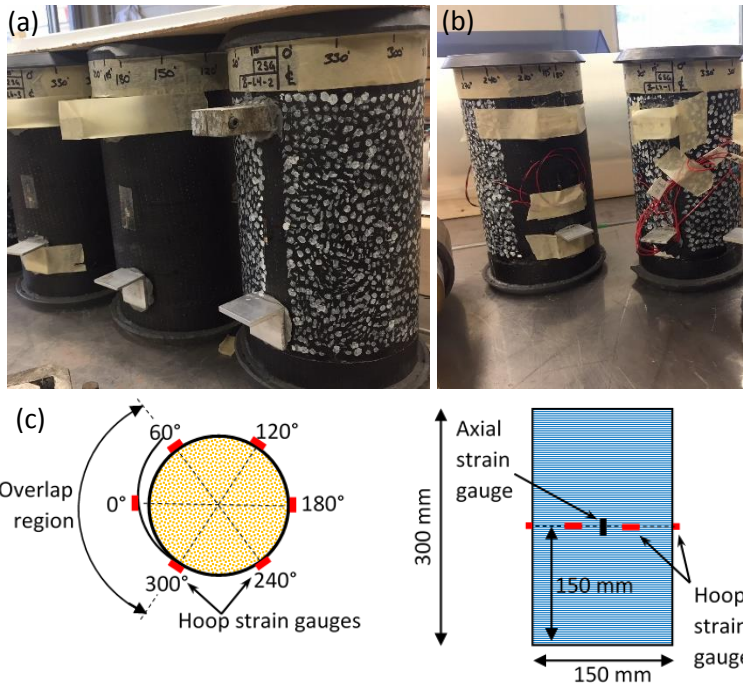
629



630

631 **Figure 1. Material testing of BFRP coupons: (a) stress-strain behavior; (b) testing machine;**
 632 **and (c) strain gauged coupon.**

633



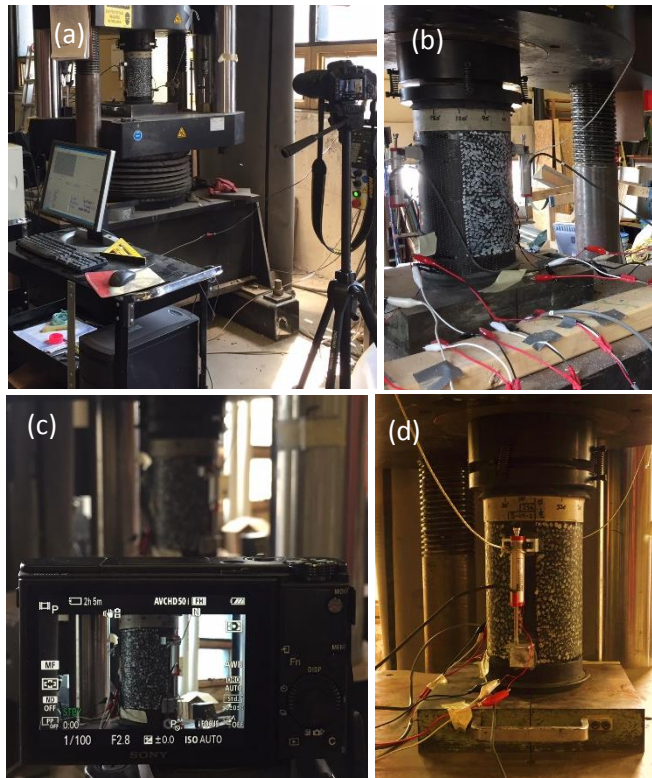
634

635

636 **Figure 2. Specimen preparation and instrumentation: (a) bracket of displacement gauges**
 637 **applied; and (b) strain gauges wired; and (c) strain gauges arrangement.**

638

639



640

641

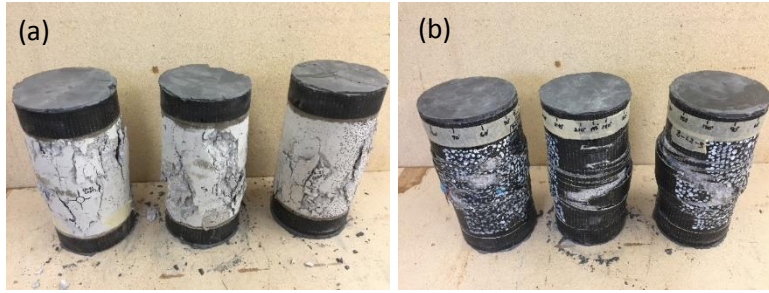
642

643

644

Figure 3. Test setup: (a) testing machine; (b) instrumentation; (c) camera; and (d) displacement gauge.

645



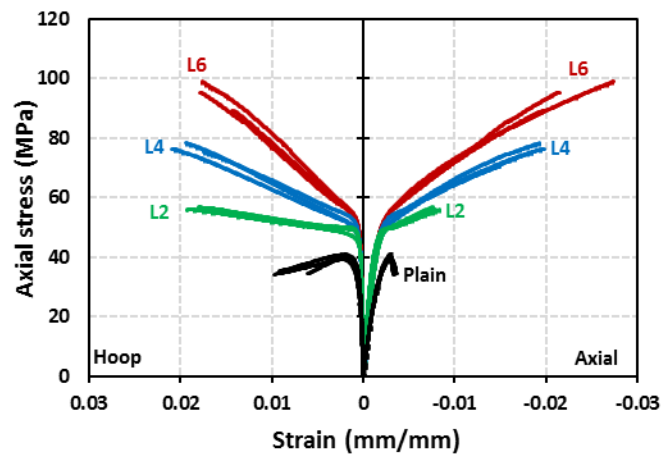
646



647



648 **Figure 4. Test specimens after failure: (a) plain group; (b) L2 group; (c) L4 group; (d) L6**
649 **group; (e) and (f) typical rupture of hoop fibers.**
650

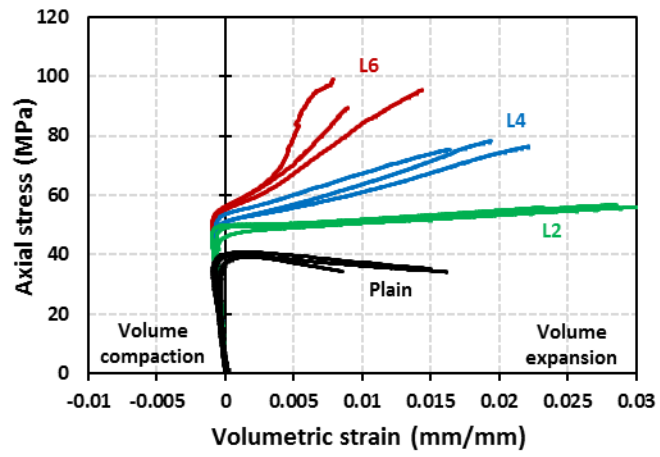


651

652

Figure 5. Stress-strain behavior of specimens.

653

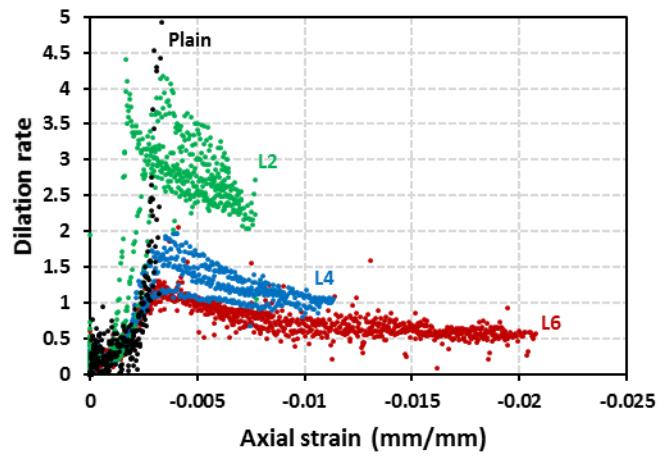


654

655

Figure 6. Variation of volumetric strain of specimens.

656

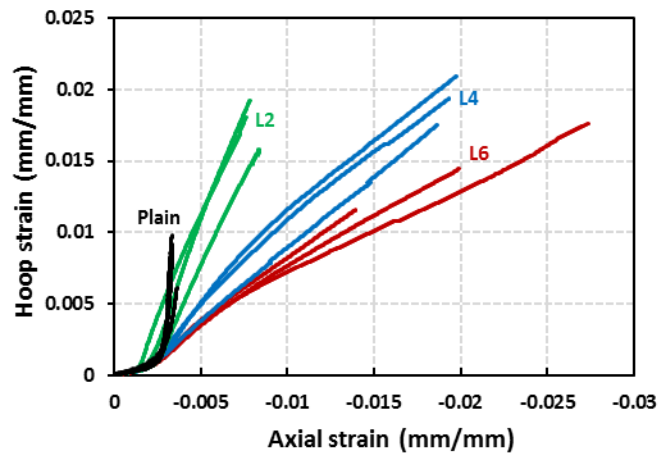


657

658

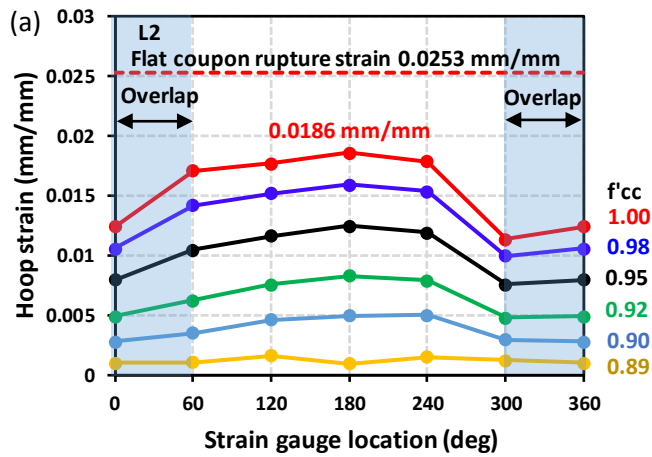
Figure 7. Variation of dilation rate vs. axial strain of specimens.

659

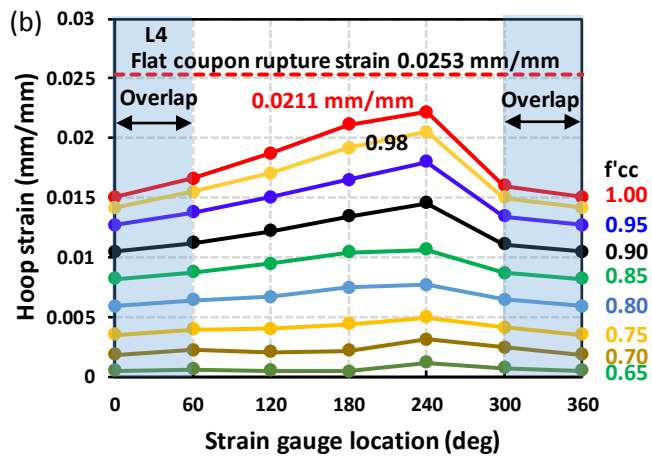


660
 661
 662

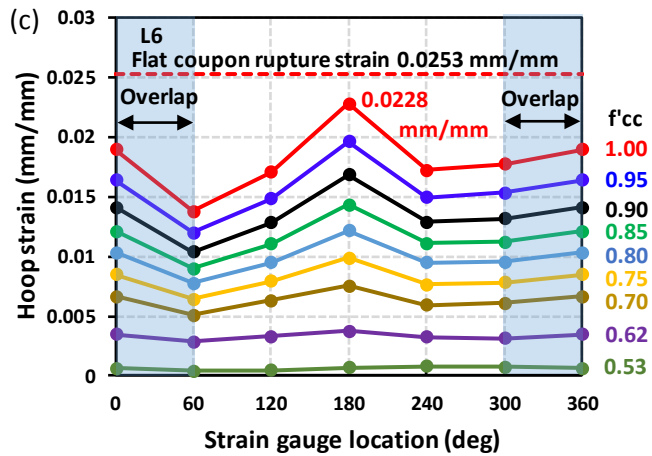
Figure 8. Variation of hoop strain vs. axial strain of specimens.



663



664



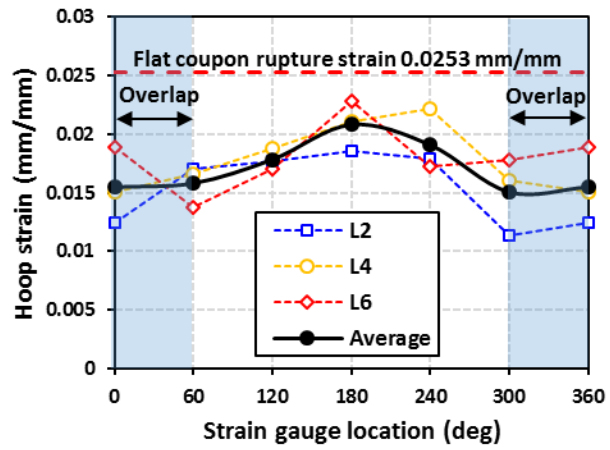
665

666

667

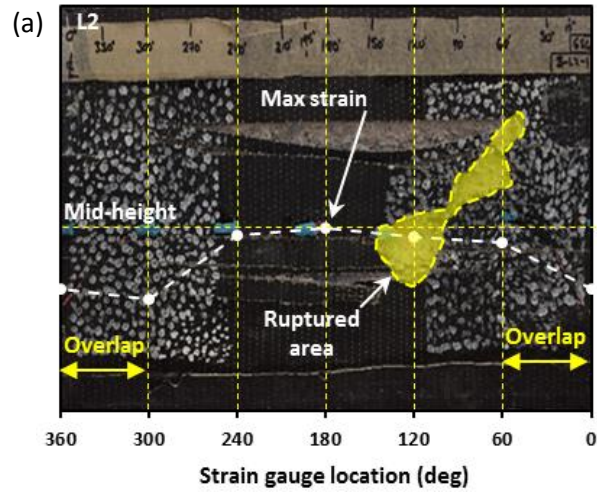
668

Figure 9. Distribution of hoop strain at mid-height of (a) L2, (b) L4, and (c) L6 specimens with six strain gauges.

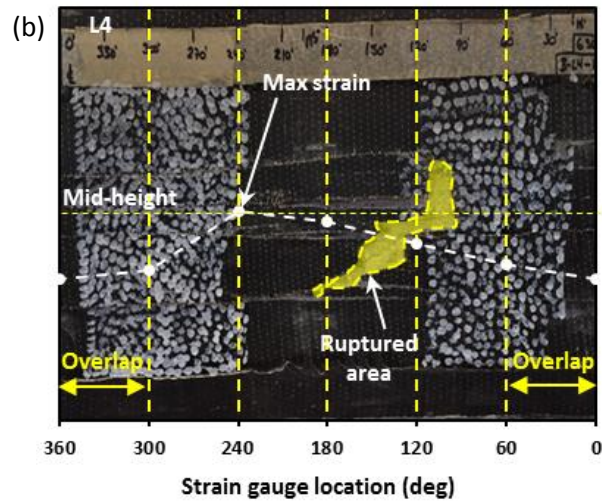


669

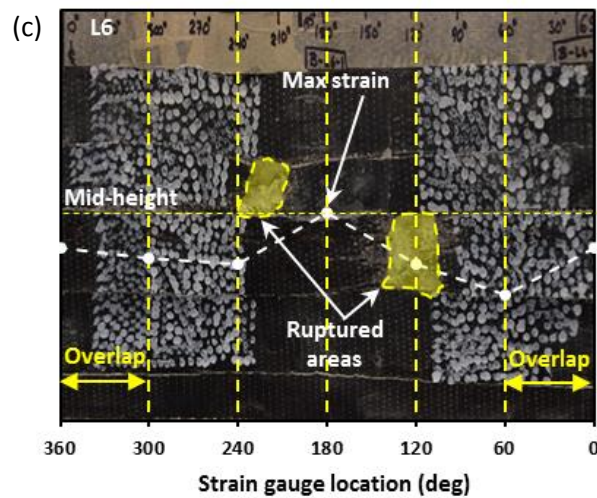
670 **Figure 10. Effect of number of BFRP layers on distribution of hoop strain at peak load.**



671



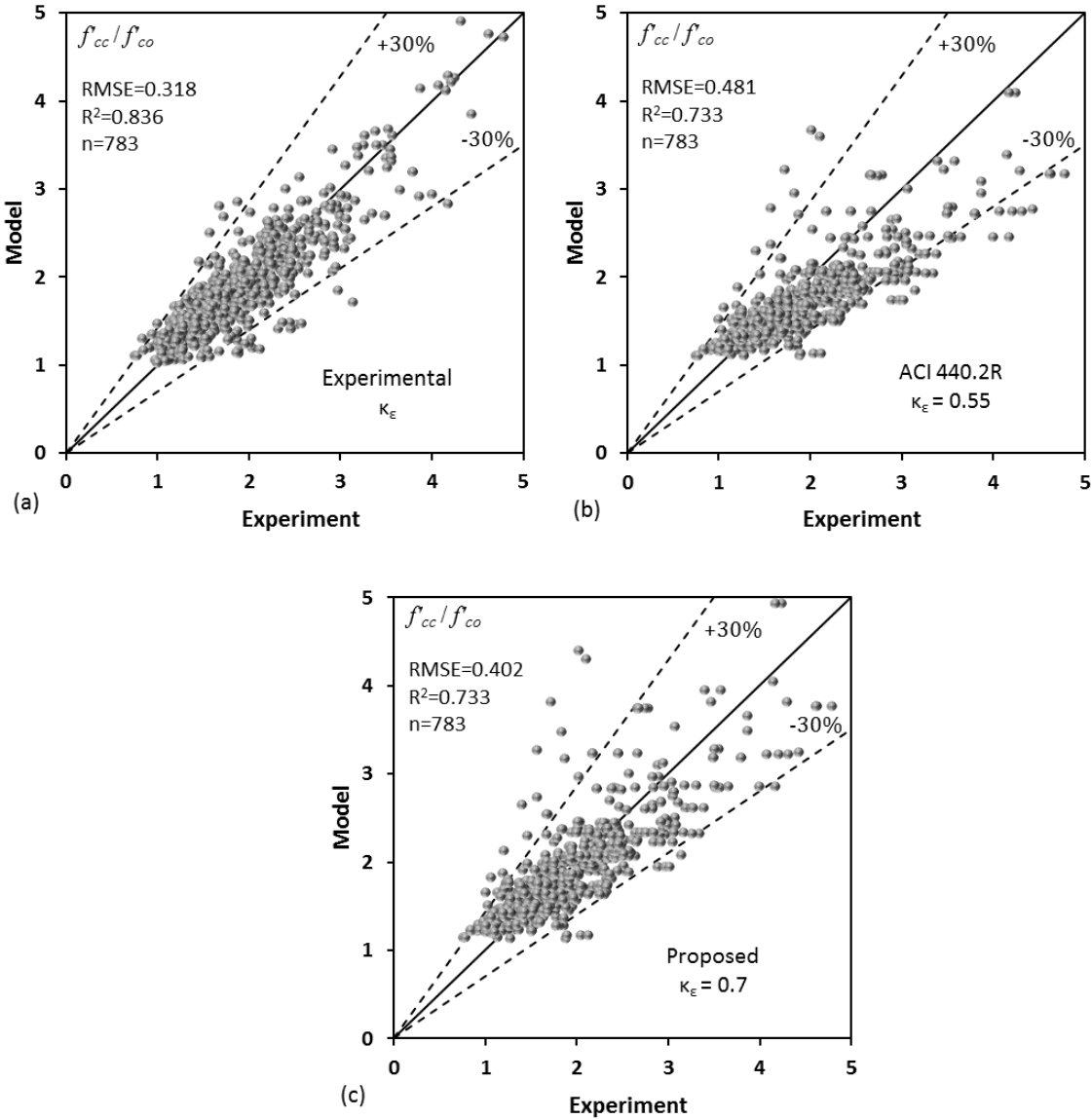
672



673

674 **Figure 11. Ruptured areas of BFRP wrap compared with hoop strain distribution of (a) L2,**
 675 **(b) L4, and (c) L6 specimens with six strain gauges.**

676

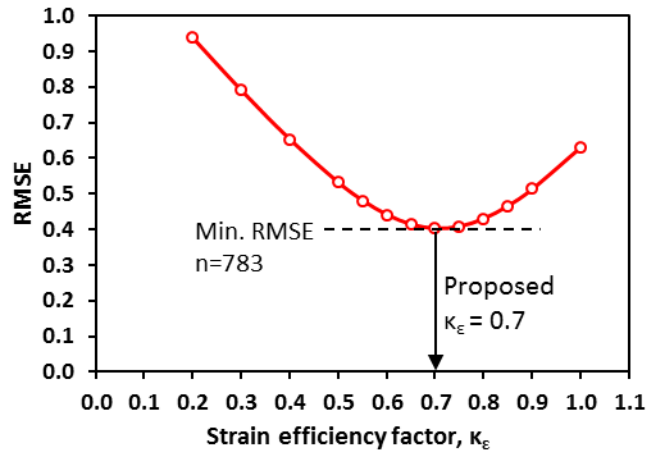


677

678

679 **Figure 12. Performance of Lam and Teng [37] confinement model prediction f'_{cc}/f'_{co} using:**
 680 **(a) experimental strain efficiency factor; (b) ACI 440.2R-17 [45] strain efficiency factor of**
 681 **0.55; and (c) refined strain efficiency factor of 0.70.**

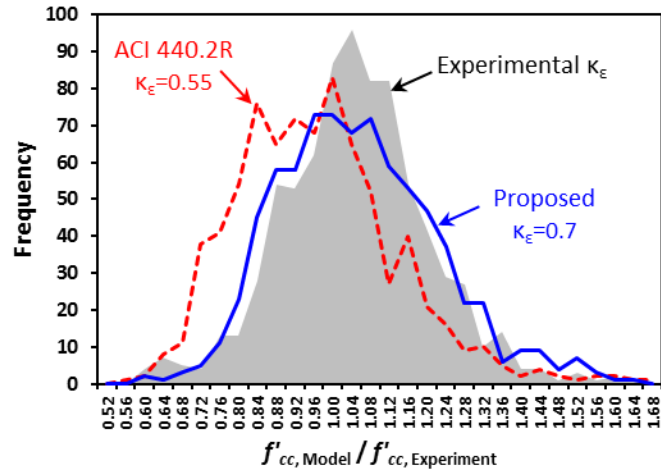
682



683

684 **Figure 13. Calibration of a strain efficiency factor based on the performance of Lam and**
 685 **Teng [37] confinement model using 783 test data.**

686



687
 688
 689
 690
 691

Figure 14. Frequency distribution of the f'_{cc} (model) to f'_{cc} (experiment) based on experimental, ACI 440.2R, and proposed strain efficiency factor using 783 test data.